An Accurate and Robust Region-Growing Algorithm for Plane Segmentation of TLS Point Clouds Using a Multiscale Tensor Voting Method

Hao Wu, Xiang Zhang, Wenzhong Shi, Shaoxian Song, Abraham Cardenas-Tristan, and Kui Li

***Abstract*—The accuracy and robustness of plane segmentation using a region-growing algorithm remains an important and challenging topic for terrestrial laser scanning point clouds. The plane segmentation of a region-growing algorithm depends heavily on the seed point, as there are currently no universally valid criteria. This article proposes a multiscale tensor voting method (MSTVM) to determine the appropriate seed point for the region-growing algorithm. A comprehensive plane strength indicator calculated by the semivariogram model has been established to assess whether a certain point is suitably considered as a seed point or not. A point cloud containing 17,881 points in a 400-m^2 area was selected to validate the proposed algorithm. The results suggest that the scale range calculated by the semivariogram model can effectively mitigate the scale effect of the tensor voting method (TVM). The comprehensive plane strength of our proposed algorithm in seed point determination is shown to be more salient than the principal component analysis and the TVM. The findings further reveal that the utility of the MSTVM-based region-growing algorithm can achieve more accurate plane segmentation results and perform with better robustness in noisy point clouds. This allows our proposed method to be more widely applied to complex real situations.**

***Index Terms*—Multiscale tensor voting method (MSTVM), plane segmentation, region-growing algorithm, seed point determination, semivariogram, terrestrial laser scanning (TLS).**

Manuscript received April 21, 2019; revised July 17, 2019; accepted August 15, 2019. This article was supported in part by the National Natural Science Foundation of China under Grant 41671406, in part by the Hubei province technical innovation special major project under Grant 2019ACA143, in part by the National Key Research and Development Program of China under Grants 2018YFC0810600 and 2017YFE0109500, and in part by the Hubei Provincial Natural Science Foundation of China under Grant 2016CFA013. *(Corresponding author: Hao Wu.)*

H. Wu is with the College of Urban and Environmental Sciences, Central China Normal University, Wuhan 430079, China, and also with the Hubei Provincial Key Laboratory for Geographical Process Analysis and Simulation, Central China Normal University, Wuhan 430079, China (e-mail: haowu1977@163.com).

X. Zhang, S. Song, and K. Li are with the School of Resource and Environment Engineering, Wuhan University of Technology, Wuhan 430070, China (e-mail: xiangzhang1992@126.com; ssx851215@whut.edu.cn; 2249732583@qq.com).

W. Shi is with the Department of Land Surveying and Geo-Informatics, The Hong Kong Polytechnic University, Hunghom, Kowloon, Hong Kong 999077, China (e-mail: wenzhongshi1963@163.com).

A. Cardenas-Tristan is with the Faculty of Engineering-Geomatics Engineering, Autonomus University of San Luis Potosí 78290, Mexico (e-mail: abraham.cardenas@uaslp .mx).

Color versions of one or more of the figures in this article are available online at http://ieeexplore.ieee.org.

Digital Object Identifier 10.1109/JSTARS.2019.2936662

I. Introduction

TERRESTRIAL laser scanning (TLS), as a new measurement method, has recently been widely used in many industries, including deformation monitoring [1], [2], cultural heritage management [3], urban planning [4], and building reconstruction [5]–[8]. Especially for building reconstruction, more comprehensive building information about facades can be obtained from TLS, which provides more perfect geometry information than that obtained from airborne laser scanning [9], [10]. Although building structures are becoming increasingly complicated, it is feasible to use TLS to identify various planes and then aggregate them for model reconstruction [11]. Plane segmentation has become an important topic that divides three-dimensional (3-D) point clouds into different planes according to certain selection standards.

Plane segmentation dates back to parameter-based methods, which check the candidate shapes against all points and then locate the exact point position with the best fit [12], [13]. The method has demonstrated good robustness given the constraints of the candidate models, but there is still the unacceptable restriction of the need to generate many spurious planes to perform plane segmentation with less accuracy [14]. Yang and Dong addressed this problem by proposing a shape-based segmentation method for large-scale mobile laser point clouds, which provides good accuracy and computationally effective time costs [15]. Since 2002, clustering-based methods have achieved plane segmentation by aggregating points having the same characteristics more accurately than parameter-based methods. This approach is less robust because the computation procedures for point features suffer seriously from neighborhood size and data noise. Recently, region-growing-based methods that require a small number of seed points and fewer criteria are increasingly being used in plane segmentations. Schuster also successfully segmented a building facade from TLS point clouds [16]. Nurunnabi *et al*. combined region growing and fast minimum covariance determinant to complete plane segmentation in highly noisy point clouds [17]. Garcia-Selles *et al*. innovatively attempted to study near-planar geological plane segmentation by region growing from outcrop data for geological analysis [18]. Vo *et al*. introduced an octree-based region-growing algorithm for the fast plane segmentation of 3-D point clouds [19]. Despite these significant contributions to region growing for achieving plane segmentation, no substantial research has yet been attempted to

increase the accuracy and robustness under the circumstance of complex scenes with multiple objects. In particular, the problem of seed point selection without universally valid criteria has been a critical constraint on the accuracy and robustness of plane segmentation using a region-growing algorithm [20], [21].

Many effective algorithms for seed point selection have been outlined to improve region growing. The classic algorithm is to employ the minimum curvature for selection of the seed point [22], [23]. Due to the emergence of this concept, recent research showing examples of newly developed techniques for seed point selection is available [24]. Vieira and Shimada removed points along sharp edges using a curvature threshold and selected the remaining points in the interior region as seed points [25]. Gorte performed a region-growing segmentation using a triangular irregular network as the seed surface [26]. Another important approach for finding the appropriate seed point is principal component analysis (PCA), which relies on local surface saliency features [27]–[29]. Roggero formulated an inertia tensor, followed by encoding the principal component of this tensor at each point by linear transformation, in which the minimum eigenvalue of the tensor was chosen as the basis for selecting seed points [30]. Recently, the tensor voting method (TVM), using a voting methodology for inferring features from discrete random data, has been used frequently to perform segmentation in a feature space [31]. One important advantage of TVM is that all geometric structures (including surfaces, lines, and points) can be inferred simultaneously, and the method also provides additional information about the strength of features. Schuster selected seed points from eigenvalues and eigenvectors of TVM and then developed a new region-growing method [16]. Lin and You presented a cluster method of planar normal vectors to classify planar features using TVM [32]. Both of these methods demonstrated an obvious problem: the second-order tensor representation of TVM for each point is affected by a certain number of its neighboring points. Once the number of neighboring points is too small, the geometric information is insufficiently collected from neighboring points. Conversely, the error information from a discrete point is transmitted into the tensor when the number of neighboring points is too large [33]. Gumhold *et al*. applied small scale when extracting the planar features of fine point cloud data and gets good results [34]. While Mark's work indicates that such small scale cannot guarantee the robustness for point clouds with noise [35]. Lin *et al*. proved that the small area with obvious plane feature would be filtered out with large scale setting [36]. It is thus necessary to propose an improved algorithm to reduce the above scale effect for choosing the most appropriate seed point such that we can enhance the accuracy and robustness of region growing.

The objective of this article is to propose the multiscale TVM (MSTVM) for improving the selection of seed points in region growing for plane segmentation. In this method, we adopt the exponential semivariogram model to determine the scale range, rather than a certain scale, to reduce the influence of a single scale. This allows us to obtain more comprehensive plane segmentation results and performs well in noisy point clouds using region growing.

II. Methods

A. TVM-Based Seed Point Determination

Seed point determination is the first step in the region-growing method, which identifies the initial location of regional spread for ensuring correctness of the regional characteristic structure. There are many evaluation algorithms for evaluating seed points, among which the TVM is a state-of-the-art method because it is model free and noniterative. For each point, its integrated tensor collects all of the votes cast within its neighborhood and is decomposed as shown below

$$T = (\lambda_1 - \lambda_2)\left(v_1 v_1^T\right) + (\lambda_2 - \lambda_3)\left(v_1 v_1^T + v_2 v_2^T\right) + \lambda_3\left(v_1 v_1^T + v_2 v_2^T + v_3 v_3^T\right) \quad (1)$$

where T is an integrated tensor. v_1, v_2, and v_3 are the decomposed eigenvectors whose corresponding eigenvalues are λ_1, λ_2, and λ_3, respectively.

According to the spectrum theorem [31], different combinations of these three eigenvalues can represent various local features as follows.

1) If λ_2 is less than λ_1 but is approximately equal to λ_3, the local structure of the seed point is characterized as a typical plane; we can use $\lambda_1 - \lambda_2$ and v_1 to describe its strength and the normal vector, respectively.
2) If λ_2 is greater than λ_3 but is approximately equal to λ_1, then the local structure of the seed point is characterized as a typical curve; we can use $\lambda_2 - \lambda_3$ and v_3 to describe its strength and the tangent vector, respectively.
3) If λ_1, λ_2, and λ_3 are roughly equal, then the local structure of the seed point is characterized as a typical point; we can use λ_3 to describe its strength. Therefore, $\lambda_1 - \lambda_2$, $\lambda_2 - \lambda_3$, and λ_3 can be regarded as the feature strength indicators for planes, curves, and points, respectively.

To perform the plane segmentation from TLS point clouds based on case 1), we need to nondimensionalize $\lambda_1 - \lambda_2$ for clarity of analysis. According to [33], the plane feature strength is expressed by standardization as follows:

$$\varphi_1 = (\lambda_1 - \lambda_2)/\lambda_1 \quad (2)$$

where φ_1 is the plane feature strength. For a given point, when its plane feature strength is greater than a threshold value, the point can be regarded as a seed point for region growing. A detailed computation of region growing was performed by [36].

B. Proposed MSTVM of Seed Point Determination

Although the strength of plane features is feasible for distinguishing those points characterized as plane features from TLS point clouds in theory, this is heavily disturbed by the vote number in practice. Min *et al.* demonstrated that both λ_1 and λ_2 are strongly related to the vote number and defined it as the scale [33]. The scale variation (i.e., differences in the vote number) often leads to large changes in the plane feature strength, that is, scale effect in nature. For example, a small scale may perform well in a fine point cloud, but its plane feature calculation results are not reliable for actual engineering that easily results in point clouds with many noises. Conversely, a large scale might not

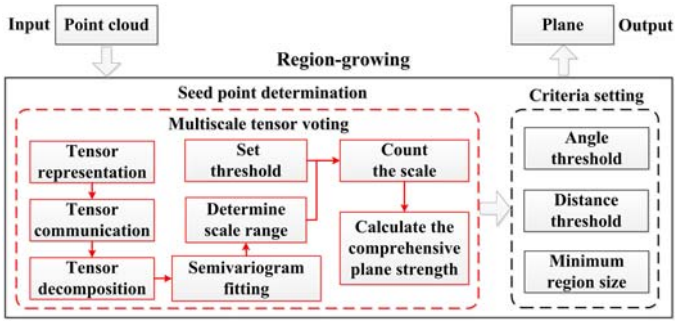

Fig. 1. Flowchart for plane segmentation of a TLS point cloud using the MSTVM.

detect certain plane features if the plane area is smaller than the search region. It is very difficult to establish an appropriate scale for determination of the seed point under the circumstances of unknown measurement data. To solve this problem, we propose an MSTVM for determining the appropriate seed point to perform plane segmentation of TLS point clouds with accuracy and robustness. It can give us the scale range so as to effectively decrease the influence of a single scale. This proposed method makes use of statistical probabilities based on multiple samples at different scales to calculate a new evaluation value, followed by determination of whether a certain point is suitable as a seed point. For a specific point, its statistical probability refers to the comprehensive plane strength, which is calculated under different scales. This reduces the scale effect resulting from different point densities and neighborhood sizes. The overall procedure for this method is shown in Fig. 1.

Step 1. Apply the TVM (including representation, communication, and decomposition) to calculate the plane strength of each input point. During the communication of the TVM, we should use varying numbers of votes to obtain plane strengths for different scales.

Step 2. View scales and their standard deviations of plane strength as regionalized variables and dependent variables, respectively. We then use the semivariogram to calculate the scale range. A detailed process of semivariogram was explained by Onyejekwe *et al.* [37].

Step 3. Set the threshold for plane feature strength and count the scale that is greater than the threshold. We then calculate the comprehensive plane strength and use it to determine seed points.

Step 4. According to various criteria, including the angle threshold, the distance threshold, and the minimum region size, we use these seed points to perform the plane segmentation

Suppose there is an unstructured point cloud that is composed of *n* points containing only spatial information and is defined as $P = \{p_i \in R^3 | i = 1, 2, \ldots, n\}$. For a given point i, we obtain its plane feature strengths for different scales, then organize these into a vector as follows:

$$\varphi_i = (\varphi_{i1}, \varphi_{i2}, \ldots, \varphi_{im}) \tag{3}$$

where m is the number of the scale. For all points, an integrated matrix is constructed.

$$\varphi = \begin{bmatrix} \varphi_1 \\ \vdots \\ \varphi_n \end{bmatrix} = \begin{bmatrix} \varphi_{11} & \cdots & \varphi_{1m} \\ \vdots & \ddots & \vdots \\ \varphi_{n1} & \cdots & \varphi_{nm} \end{bmatrix} \tag{4}$$

where φ is an integrated matrix. To perform the determination of seed points more clearly, the elements in φ are marked out to whether or not they can represent a plane as shown below

$$\varphi'_{ij} = \begin{cases} 1 & \varphi_{ij} \geq \xi \\ 0 & \varphi_{ij} < \xi \end{cases} \tag{5}$$

where φ'_{ij} is the label value of p_i at scale j. ξ is the threshold of plane feature strength and only the points with the planar feature strength greater than ξ can be regarded as seed points. A detailed process of setting the value of the parameter ξ, 0.94, was explained by [36]. The comprehensive plane strength is calculated as follows:

$$\varphi'_i = \left(\sum_{j=1}^{m} \varphi'_{ij} \right) \Big/ m \tag{6}$$

where φ'_i is the comprehensive plane strength of p_i . The point having the largest $\varphi'_i - \text{value}$ is selected as the first seed point for region growing. The region for growing is extended from this seed point to neighboring points. For a certain point, if the $\varphi'_i - \text{value}$ of the point is greater than ξ, and the difference of the normal vector between the point and the seed point is less than the threshold of the direction difference, this point is merged into the region. Otherwise, we ignore this point. Likewise, for the rest of the point cloud, the point with the largest $\varphi' - \text{value}_i$ is used as a new seed point for growth of the next region. This region-growing procedure proceeds until no more seed points are available.

C. Scale Range Identification of MSTVM Using Semivariogram

The scale range identification of MSTVM is an essential prerequisite for us to perform the MSTVM. The semivariogram is used to determine the scale range because it has an advantage for modeling the spatial variability of each variable [38]. It is useful for us to determine the appropriate scale range, as there is a strong spatial correlation between a seed point and its neighboring points [31]. The semivariogram is a function related to the semivariance, with a regionalized variable increment as follows:

$$\gamma(h) = \frac{1}{2N(h)} \sum_{i=1}^{2N(h)} [Z(x_i + h) - Z(x_i)]^2 \tag{7}$$

where $\gamma(h)$ is the semivariogram value; h is the lag of distance; $N(h)$ is the set of all pairwise Euclidean distances; and $Z(x_i + h)$ and $Z(x_i)$ are variable values at spatial locations $x_i + h$ and x_i, respectively. Fig. 2(a) shows that the standard semivariogram curve is plotted with the lag of distance, h, on the *x*-axis and semivariogram value, $\gamma(h)$, on the *y*-axis. It can

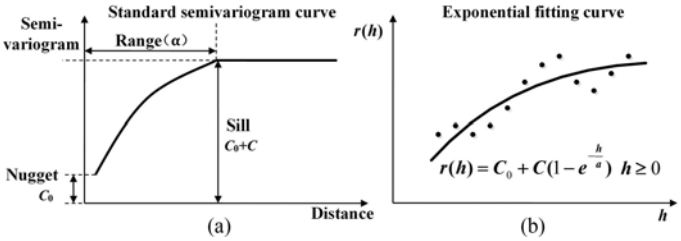

Fig. 2. Curves of standard semivariogram and exponential model.

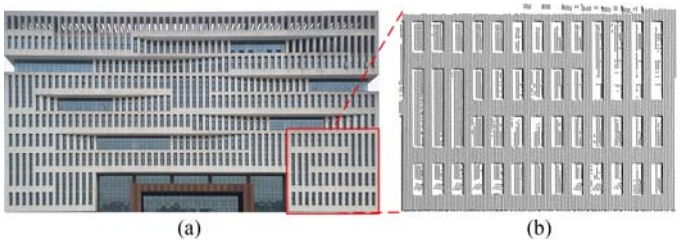

Fig. 3. Photographs of building and point cloud data.

directly express the spatial variation process and characteristics. The shape and structure of the curve are determined by three parameters, including nugget C_0; sill $C_0 + C$; and range a. Nugget C_0 indicates the measurement error of the variable. Sill $C_0 + C$ explains the structural variance of the variable itself. Range a is the spatially dependent range of the variable. Within range a, the closer point pairs have similar characteristics, and the spatial correlation between observations at any two points decreases with an increase of h.

There are many semivariogram models for different types of observed data. Fig. 2(b) shows the exponential model that we used for our experimental data

$$\gamma(h) = C_0 + C\left(1 - e^{-\frac{h}{b}}\right) \tag{8}$$

where b is a constant associated with range. According to [38], range is equal to $3b$ when the semivariogram $\gamma(h)$ reaches 95% of the sill value, $C_0 + C$. When h approaches $3b$, the maximum spatial difference will be stable at sill $C_0 + C$. With further expansion of h, the spatial correlation remains fundamentally unchanged, and the semivariogram value approximates a horizontal line. For seed point determination using our proposed MSTVM, h determines the search region of vote process. When h increases to $3b$, the plane feature strength can be more accurately calculated since the search region and the detection plane are essentially the same size. Due to the difference of plane size in a real point cloud, we select a neighborhood that is centered on $3b$ as the appropriate scale range for the MSTVM.

III. Data

The building used in this experiment is the Nanhu Library of Wuhan University of Technology shown in Fig. 3. The library dimensions are 80 m in length, 70 m in width, and 55 m in height. Its front side contains many types of vertical and horizontal planes. Most of the planes are small in width and are closely spaced. The outer structure of the entire library is made of steel. Due to the building's load-bearing and external environment, there are risks such as deformation and rust in the lower-left corner and in the lower-right corner of the library, which are the most vulnerable parts. Periodic examinations of the deformation of these two corners are required by detecting plane structures. Fig. 3(a) shows a front photograph of the library.

Point cloud data were acquired using Leica ScanStation P40 3-D laser scanner. The laser scanner was placed in front of the building to collect the front data of the library at a scanning resolution of 6.3 mm/10 m. We captured a 400-m^2 area located at the lower-right corner of the library in Cyclone@ Leica 9.1 as the experimental data. The experimental data contain 17,881 points and many types of vertical and horizontal planes, including protruding concrete walls, glass windows recessed from the frame, extended platforms, and other structures. Fig. 3(b) shows an overview of the experimental data.

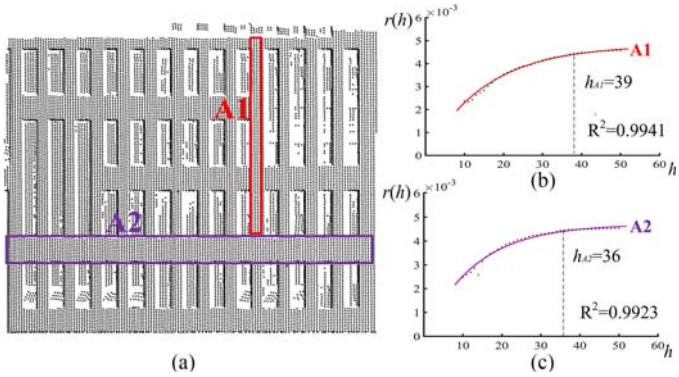

Fig. 4. Identification results of the scale range of MSTVM using the semivariogram.

IV. Results

The entire segmentation experiment process consists of two main results: 1) the scale range results for multiscale tensor voting and 2) a description of the experimental results.

A. Results of Appropriate Scale Range of MSTVM

Each point in the study data set can be represented a second-order symmetric tensor. The initial scale range is set from 10 to 50 in process of tensor communication. The plane feature strengths for two sample areas (A1 and A2) at 41 scales are decided by tensor decomposition, respectively. Then, we fit both semivariograms according to the plane feature strength. Fig. 4 shows the results of the appropriate scale range of MSTVM using the semivariogram. There are two sample areas (A1 and A2), shown in Fig. 4(a), representing the vertical and horizontal planes, respectively. Fig. 4(b) and (c) shows the fitting curves using the semivariogram exponential model corresponding to A1 and A2. It suggests that each exhibits an upward trend with an increase in scale and a good fit with the coefficient of determination R2, 0.9941 and 0.9923, close to 1. The ranges h_{A1} and h_{A2} are 39 and 36, respectively, which provide a

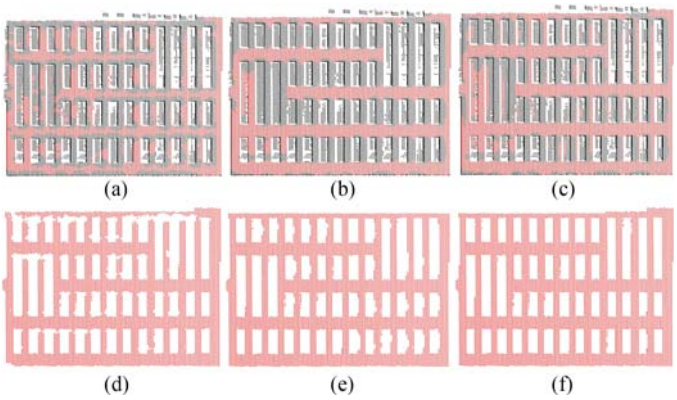

Fig. 5. Results of seed point identification and the corresponding plane segmentation results using the region-growing algorithm.

quantitative reference of the appropriate scale range for the experimental data. The mean of range h_{A1} and range h_{A2} is 38 and is viewed as the middle value of an appropriate scale range for MSTVM. The identification of the appropriate scale range is required not only to take various geometric features of the study area into consideration but also to avoid the situation of a sharply increased calculation load due to an excessive scale range. In this case, the extent of the appropriate scale range is approximately half that of the initial scale range. For this experiment, because the total of the initial scale range is 40, the extent of the appropriate scale range is 20. Finally, considering the fact that the center value of the appropriate scale range discussed above is 38, the appropriate scale range of MSTVM can be determined as 28 and 48.

B. Results of Plane Segmentation Using the Region-Growing Algorithm

We count the scales that are greater than the threshold set 0.94 under the appropriate scale range. The comprehensive plane strength of MSTVM is calculated by (6) and used to determine seed point as shown in Fig. 5(c). Fig. 5(a), (b), and (c) shows the results of seed point determination using PCA, TVM, and MSTVM, respectively (red marked dots represent seed points). According to the rule of [30], where a given point with a minimum eigenvalue less than 0.1 can be attributed to a seed point, the seed point result shown in Fig. 5(a) is obtained using point cloud library (PCL) 1.8.0. For TVM and MSTVM, those points with plane feature strengths greater than 0.94, as shown in Fig. 5(b) and (c), are defined as seed points using MATLAB R2014a@MathWorks. The number of seed points for PCA, TVM, and MSTVM is 5993; 6318; and 7402, respectively. It is clear that the number of seed points from PCA is significantly smaller than that of both TVM and MSTVM. Furthermore, the ability to identify seed points for MSTVM is better than that for TVM. For region growing, the size of the minimum region is 1000. The neighboring points are merged into the region if the distance from the neighboring points to the tangent plane of the seed point is less than the distance threshold, and the difference of the normal vector between the neighboring points and the seed point is less than an angle threshold of 10°. According to these criteria, Fig. 5(d), (e), and (f) shows that the final plane segmentation results based on the above seed points from PCA, TVM, and MSTVM, respectively, are obtained using the region-growing algorithm. It is evident that the plane segmentation effect of MSTVM is more complete than that of PCA and TVM.

If the appropriate scale range is not determined in advance, the segmentation can only be performed under a certain scale by experience. For example, Fig. 5(d) and (e) shows the segmentation results by PCA and TVM method at scale 45 and 30, respectively, of which the segmentation effects are not as good as in Fig. 5(f). It proves that using the semivariogram to decide the appropriate scale range is a good suggestion. In addition, the coefficient of determination R2 for the exponential model curves in Fig. 4(b) and (c) are 0.9941 and 0.9923, respectively. According to statistical principles, a good fit has an R2 close to 1. Therefore, we choose exponential model to fit semivariogram to detect the appropriate scale range.

V. Discussion

In this section, we will discuss the superiority of MSTVM, particularly its accuracy and robustness.

A. Saliency of Plane Feature Strength for Our Proposed MSTVM

Identification of seed points is a prerequisite for plane segmentation. Our proposed MSTVM provides a new plane feature strength indicator that is characterized by saliency to produce a more intuitive determination of seed points. To comprehensively demonstrate the superiority of this indicator, we marked three segments, L1, L2, and L3, with different combinations of walls and windows in the initial point cloud data shown in Fig. 6(a). Fig. 6(b), (c), and (d) shows the plane feature strengths of L1, L2, and L3 as calculated by PCA, TVM, and MSTVM, respectively. For the large area on the left-hand side of L1, shown in Fig. 6(a), and its plane strength as calculated by PCA, shown in Fig. 6(b), is close to 0; its plane strength values calculated by TVM and MSTVM [shown in Fig. 6(c) and (d)] are both close to 1. These results from PCA, TVM, and MSTVM are in agreement with the rules for seed point determination reported by [29] and also in agreement with those of [33]. However, for the small area on the right side of L1, the amplitude variation of plane feature strength between plane points and nonplane points in MSTVM (from 0 to 1) is larger than for TVM (from 0.2 to 1) and for PCA (from 0 to 0.2). This result suggests that MSTVM is more suitable for working with small areas than is PCA or TVM.

Larger amplitude changes are more intuitively distinguished as seed points from a TLS point cloud than are small amplitude changes. In addition, for the small plane on the right-hand side of L1, the troughs shown in the right-hand side of Fig. 5(b) represent seed points identified by PCA, while the peaks shown in the right-hand side of Fig. 5(c) and (d) represent seed points identified by TVM and MSTVM. Although there are three planes with same width on the right-hand side of L1, the widths of both troughs in PCA and the peaks in TVM are different. This

TABLE I
SUMMARY OF SEGMENTATION RESULTS UNDER PCA, TVM, AND MSTVM

Reference Data					Accuracy Metric			
	Method	Class	PP	NPP	Segmentation Accuracy	Kappa Coefficient	Commission Error	Omission Error
Region Growing	PCA	PP	10713	2387	93.50%	0.597	22.20%	7.00%
		NPP	747	4034				
	TVM	PP	10987	3053	95.90%	0.53	27.80%	4.30%
		NPP	473	3368				
	MSTVM	PP	11130	2293	97.10%	0.658	20.60%	3.00%
		NPP	330	4128				

PP: Plane Point
NPP: Nonplane Point

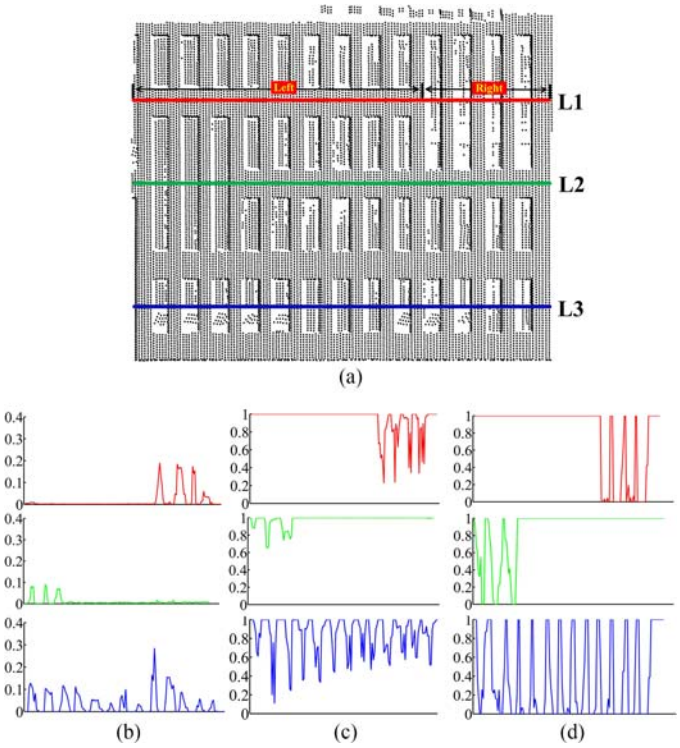

Fig. 6. Three different segments and their plane feature strengths. (a) Location of three segments L1, L2, and L3 on the cloud point data and variation of plane feature strength at each point on the segments L1, L2, and L3 calculated based on (b) PCA, (c) TVM, and (d) MSTVM.

suggests that the saliency of the seed point area identified by PCA and TVM shows large fluctuations. However, the width of the peaks in MSTVM is very uniform, and the number of peaks corresponds to the small plane in the point cloud shown in Fig. 5(a). The same phenomenon also exists in L2 and L3. This indicates that MSTVM is more salient to calculate the plane feature strength than PCA and TVM.

B. Accuracy Assessment of Plane Segmentation

An accuracy assessment of plane segmentation is conducted by validating the rationality of seed points obtained from our proposed MSTVM. The reference data, including the plane points and the nonplane points, are produced in CloudCompare@ EDF R&D. We selected a series of accuracy metrics, which include segmentation accuracy, kappa coefficient, commission error, and omission error. Segmentation accuracy is a statistic that represents the probability of the plane point being correctly classified. The kappa coefficient is a measure of how well the classification results and the associated reference data agree. Commission errors occur when nonplane points are erroneously included in the plane class. Omission errors occur when plane points that should have been included in the plane class are included in other classes. A detailed computation of above four accuracy metrics was performed by [39]. Table I shows the accuracy assessment of the plane results and is segmented by the region-growing algorithm for the case of three groups of seed points, as shown in Fig. 5(a), (b), and (c). Table I shows that the segmentation accuracy of MSTVM is 97.10% and is followed by a TVM accuracy of 95.90% and a PCA accuracy of 93.50%. MSTVM yields the highest kappa coefficient (0.658), followed by PCA (0.597), and TVM (0.53). Both commission and omission error values for MSTVM (20.60% and 3.00%) are consistently lower than those for PCA (22.20% and 7.00%) and TVM (27.80% and 4.30%). These results indicate that better classification accuracy can be obtained when MSTVM is used to select the seed point. This result is in agreement with the results shown in Fig. 5: the segmentation result using MSTVM is more accurate than results from PCA or TVM. Compared with the segmentation results shown in Fig. 5(f), it is clear that the segmentation results using PCA shown in Fig. 5(d) miss many points at the intersections of different planes, and the segmentation results using TVM shown in Fig. 5(e) exclude many points at the edge of vertical planes. This is primarily due to the fact that the seed points identified by MSTVM shown in Fig. 5(c) are more uniformly distributed than those from PCA [see Fig. 5(a)] and from TVM [see Fig. 5(b)], allowing us to achieve a better plane segmentation effect.

C. Robustness Assessment for Different Noise Levels

Due to the influence of the instrument itself and external environmental conditions, it is inevitable that noise will be contained in the point cloud data when TLS is used to scan objects. To examine the robustness of MSTVM in a complex real situation,

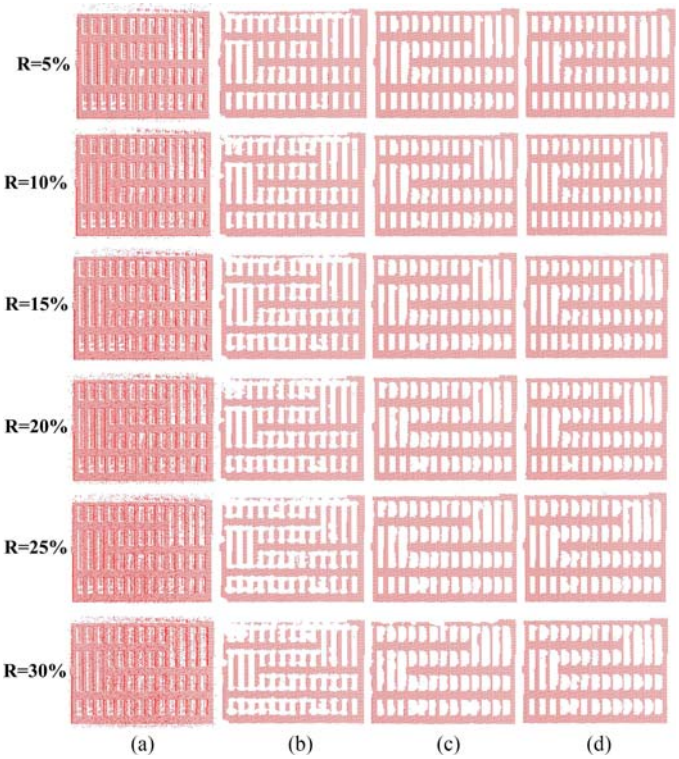

Fig. 7. Plane segmentation results of PCA, TVM, and MSTVM under different noise levels.

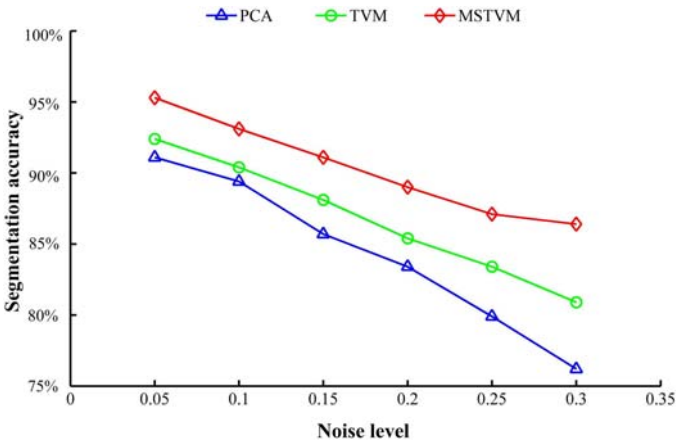

Fig. 8. Segmentation accuracy of PCA, TVM, and MSTVM under different noise levels.

we added six different levels of noise to the initial point cloud data, at levels of 5%, 10%, 15%, 20%, 25%, and 30%, as shown in Fig. 7(a). The plane segmentation results of PCA, TVM, and MSTVM are shown in Fig. 7(b), (c), and (d), respectively. These results show that all three methods are able to make appropriate plane segmentations when the noise level is 5%. However, with gradual increases of the noise ratio, the segmentation results for the three methods all gradually deteriorate, but MSTVM is less affected than other two methods. When the noise level reaches 30% (the maximum added), the planes segmented by PCA show large blank areas in which all plane points are nearly lost. The planes segmented by TVM also show different degrees of failure, while the planes segmented by MSTVM essentially have plane points remaining in all areas. Fig. 8 shows that there is an intuitive trend in segmentation accuracy under different noise levels. This suggests that the results segmented by MSTVM are more accurate than those from PCA and TVM. Furthermore, as the noise level increases from 5% to 30%, the decrease in segmentation accuracy of PCA, TVM, and MSTVM is 14.9%, 11.5%, and 8.9%, respectively. This shows that MSTVM is more stable with noise ratio changes than is PCA and TVM. The results show that MSTVM has more robust segmentation results and a higher capacity for noise tolerance in TLS point clouds.

VI. Conclusion

For terrestrial laser scanned point clouds, the region-growing algorithm is a classic plane segmentation method and is seriously affected to a large extent by seed points. Although existing research results have shown that TVM has the potential to detect distinct geometric structures, such as points, lines, and planes, determining seed points using TVM often is heavily disturbed by effects of scale (i.e., the vote number). We propose MSTVM to improve the selection of seed points in region growing for plane segmentation. The main conclusions can be summarized as follows.

1) The scale range calculated by the semivariogram model is superior to use of a single scale and can effectively mitigate the scale effect of TVM.
2) It is more feasible to use MSTVM to identify seed points than are PCA and TVM. The indicators of comprehensive plane feature strength defined by MSTVM are characterized by saliency so that we can make a more intuitive determination of seed points.
3) The utility of the MSTVM-based region-growing algorithm approach for segment planes has been shown to be more comprehensive than that of the classic methods such as PCA and TVM. Thorough analysis exhibits the superiority of our proposed algorithm with respect to accuracy and robustness.

Despite the achievements described in this article, there are several factors that need further investigation. In terms of the efficiency, our method is the same as PCA and TVM, and it may need further exploration. In addition to plane features, our proposed MSTVM can also deduce line features and point features from TLS point clouds. It is also essential to develop efficient methods to improve computational loads when using TVM.

Acknowledgment

The authors are grateful to Elsevier Language Editing Services for English-language editing of the manuscript. The authors would like to express special thanks to all the anonymous reviewers and the editor for their thoughtful and constructive comments.

REFERENCES

[1] X. J. Chen, K. G. Yu, and H. Wu, "Determination of minimum detectable deformation of terrestrial laser scanning based on error entropy model," *IEEE Trans. Geosci. Remote Sens.*, vol. 56, no. 1, pp. 105–116, Jan. 2018.

[2] H. S. Park, H. M. Lee, H. Adeli, and I. Lee, "A new approach for health monitoring of structures: Terrestrial laser scanning," *Comput.-Aided Civil Infrastructure Eng.*, vol. 22, no. 1, pp. 19–30, 2007.

[3] J. L. Lerma, S. Navarro, M. Cabrelles, and V. Villaverde, "Terrestrial laser scanning and close range photogrammetry for 3D archaeological documentation: the Upper Palaeolithic Cave of Parpalló as a case study," *J. Archaeological Sci.*, vol. 37, no. 3, pp. 499–507, 2010.

[4] J. A. Entwistle, K. J. W. McCaffrey, and P. W. Abrahams, "Three-dimensional (3D) visualisation: the application of terrestrial laser scanning in the investigation of historical Scottish farming townships," *J. Archaeological Sci.*, vol. 36, no. 3, pp. 860–866, 2009.

[5] Y. Arayici, "An approach for real world data modelling with the 3D terrestrial laser scanner for built environment," *Automat. Construction*, vol. 16, no. 6, pp. 816–829, 2007.

[6] X. Xiong, A. Adan, B. Akinci, and D. Huber, "Automatic creation of semantically rich 3D building models from laser scanner data," *Automat. Construction*, vol. 31, pp. 325–337, 2013.

[7] Z. Wang *et al.*, "A multiscale and hierarchical feature extraction method for terrestrial laser scanning point cloud classification," *IEEE Trans. Geosci. Remote Sens.*, vol. 53, no. 5, pp. 2409–2425, May 2015.

[8] Z. X. Zhang *et al.*, "A multilevel point-cluster-based discriminative feature for ALS point cloud classification," *IEEE Trans. Geosci. Remote Sens.*, vol. 54, no. 6, pp. 3309–3321, Jun. 2016.

[9] P. Shi and G. Vosselman, "Automatic extraction of building features from terrestrial laser scanning," *Int. Arch. Photogramm. Remote Sens. Spatial Inf. Sci.*, vol. 36, pp. 33–39, 2006.

[10] S. M. I. Zolanvari, D. F. Laefer, and A. S. Natanzi, "Three-dimensional building facade segmentation and opening area detection from point clouds," *ISPRS J. Photogramm. Remote Sens.*, vol. 143, pp. 134–149, 2018.

[11] E. Z. Che and M. J. Olsen, "Multi-scan segmentation of terrestrial laser scanning data based on normal variation analysis," *ISPRS J. Photogramm. Remote Sens.*, vol. 143, pp. 233–248, 2018.

[12] H. Boulaassal, T. Landes, P. Grussenmeyer, and F. Tarsha-Kurdi, "Automatic segmentation of building facades using terrestrial laser data," in *Proc. ISPRS Workshop Laser Scanning SilviLaser*, 2007, pp. 65–70.

[13] G. Vosselman, B. Gorte, G. Sithole, and T. Rabbani, "Recognising structure in laser scanner point clouds," *Int. Arch. Photogramm. Remote Sens. Spatial Inf. Sci.*, vol. 46, no. 8, pp. 33–38, 2004.

[14] T. M. Awwad, Q. Zhu, Z. Du, and Y. Zhang, "An improved segmentation approach for planar surfaces from unstructured 3D point clouds," *Photogrammetric Rec.*, vol. 25, no. 129, pp. 5–23, 2010.

[15] B. Yang and Z. Dong, "A shape-based segmentation method for mobile laser scanning point clouds," *ISPRS J. Photogramm. Remote Sens.*, vol. 81, no. 7, pp. 19–30, 2013.

[16] H. F. Schuster, "Segmentation of lidar data using the tensor voting framework," *Int. Arch. Photogramm. Remote Sens. Spatial Inf. Sci.*, vol. 23, pp. 1073–1078, 2004.

[17] A. Nurunnabi, D. Belton, and G. West, "Robust segmentation in laser scanning 3D point cloud data," in *Proc. IEEE Int. Conf. Digit. Image Comput. Techn. Appl.*, 2013, pp. 1–8.

[18] D. Garcia-Selles, O. Falivene, P. Arbues, O. Gratacos, S. Tavani, and J. A. Munoz, "Supervised identification and reconstruction of near-planar geological surfaces from terrestrial laser scanning," *Comput. Geosci.*, vol. 37, no. 10, pp. 1584–1594, 2011.

[19] A. V. Vo, L. Truong-Hong, D. F. Laefer, and M. Bertolotto, "Octree-based region growing for point cloud segmentation," *ISPRS J. Photogramm. Remote Sens.*, vol. 104, pp. 88–100, 2015.

[20] J. M. Blosca and J. L. Lerma, "Unsupervised robust planar segmentation of terrestrial laser scanner point clouds based on fuzzy clustering methods," *ISPRS J. Photogramm. Remote Sens.*, vol. 63, no. 1, pp. 84–98, 2008.

[21] O. Teboul, L. Simon, P. Koutsourakis, and N. Paragios, "Segmentation of building facades using procedural shape priors," in *Proc. IEEE Conf. Comput. Vis. Pattern Recognit.*, 2013, pp. 3105–3112.

[22] R. Adams and L. Bischof, "Seeded region growing," *IEEE Trans. Pattern Anal. Mach. Intell.*, vol. 16, no. 6, pp. 641–647, 2002.

[23] P. J. Besl and R. C. Jain, "Segmentation through variable-order surface fitting," *IEEE Trans. Pattern Anal. Mach. Intell.*, vol. PAMI-10, no. 2, pp. 167–192, Mar. 1988.

[24] J. Lerma and J. M Biosca, "Segmentation and filtering of laser scanner data for cultural heritage," in *Proc. CIPA 2005 XX Int. Symp.*, 2005, vol. 26, p. 6.

[25] M. Vieira and K. Shimada, "Surface mesh segmentation and smooth surface extraction through region growing," *Comput.-Aided Geometric Des.*, vol. 22, no. 8, pp. 771–792, 2005.

[26] B. Gorte, "Segmentation of TIN-structured surface models," in *Proc. Joint Int. Symp. Geospatial Theory Process. Appl. CDROM*, 2002, vol. 34, no. 4, pp. 465–469.

[27] T. Derose, T. Duchamp, J. Mcdonald, and W. Stuetzle, "Surface Reconstruction from unorganized points," *ACM Siggraph Comput. Graph.*, vol. 26, no. 2, pp. 71–78, 1992.

[28] A. Nurunnabi, D. Belton, and G. West, "Robust segmentation for large volumes of laser scanning three-dimensional point cloud data," *IEEE Trans. Geosci. Remote Sens.*, vol. 54, no. 8, pp. 4790–4805, Aug. 2016.

[29] M. Pauly, M. Gross, and L.P. Kobbelt, "Efficient simplification of point-sampled surface," in *Proc. Conf. Vis..*, 2002, pp. 63–170.

[30] M. Roggero, "Object segmentation with region growing and principal component analysis," *Pediatric Allergy Immunol.*, vol. 12, no. 2, pp. 59–64, 2002.

[31] G. Medioni, C. K. Tang, and M. S. Lee, "Tensor voting: Theory and applications," in *Proc. RFIA*, 2000, vol. 34, pp. 1482–1495.

[32] B. C., Lin and R. J., You, "Planar feature extraction from LIDAR data based on tensor analysis," in *Proc. 27th Asian Conf. Remote Sens.*, Ulaanbaatar, Mongolia, Oct. 9–13, 2006, pp. 1–7.

[33] K. P. Min, S. J. Lee, and K. H. Lee, "Multi-scale tensor voting for feature extraction from unstructured point clouds," *Graphical Models*, vol. 74, no. 4, pp. 197–208, 2012.

[34] S. Gumhold, X. Wang, and R. McLeod, "Feature extraction from point clouds," in *Proc. 10th Int. Mesh. Roundtable*, 2001, pp. 293–305.

[35] P. Mark and K. Richard, "Multi-scale feature extraction on point-sampled surfaces," *Comput. Graph. Forum*, vol. 22, no. 3, pp. 281–289, 2010.

[36] R. J. You and B. C. Lin. Building feature extraction from airborne lidar data based on tensor voting algorithm," *Photogrammetric Eng. Remote Sens.*, vol. 77, no. 12, pp. 1221–1231, 2011.

[37] S. Onyejekwe, X. Kang, and L. Ge, "Evaluation of the scale of fluctuation of geotechnical parameters by autocorrelation function and semivariogram function," *Eng. Geol.*, vol. 214, pp. 43–49, 2016.

[38] G. Gertner and G. Wang, "Appropriate plot size and spatial resolution for mapping multiple vegetation types," *Photogrammetric Eng. Remote Sens.*, vol. 67, no. 5, pp. 575–584, 2001.

[39] J. R. Jensen, *Introductory Digital Image Processing: A Remote Sensing Perspective*, 3rd ed. Englewood Cliffs, NJ, USA: Prentice-Hall, 2005, p. 526.

Hao Wu received the Ph.D. degree from the State Key Laboratory of Information Engineering in Surveying, Mapping and Remote Sensing, Wuhan University, Wuhan, China, in 2007.

He is a Professor with the College of Urban and Environmental Sciences, Central China Normal University, Wuhan, China. His research interests include geomatics, laser scanning and point cloud processing, and Earth observation science.

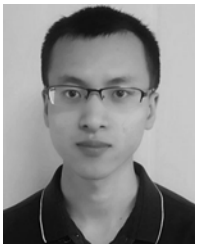

Xiang Zhang received the bachelor's degree in 2016 from the Wuhan University of Technology, Wuhan, China, where he is currently working toward the Ph.D. degree.

His current research interests include laser scanning and data processing.

Wenzhong Shi received the Ph.D. degree from the University of Osnabruck, Vechta, Germany, in 1994.

He is a Chair Professor and Head of the Department of Land Surveying and Geo-Informatics, The Hong Kong Polytechnic University, Hong Kong. His current research interests include uncertainty and spatial data quality control, point cloud processing, and GIS and remote sensing.

Abraham Cardenas-Tristan received the Ph.D. degree from the Autonomous University of Nuevo León, Nuevo León, Mexico, in 2011.

He is a Professor with the Faculty of Engineering-Geomatics Engineering, Autonomus University of San Luis Potosí, San Luis, Mexico. His current research interests include point cloud processing and deformation monitoring of mine slope.

Shaoxian Song received the Ph.D. degree from the School of Minerals Processing and Bioengineering, Central South University, Changsha, China, in 1991.

He is a Professor with the School of Resource and Environment Engineering, Wuhan University of Technology, Wuhan, China. His current research interests include deformation monitoring of mine slope.

Kui Li received the bachelor's degree from Changzhou University, Changzhou, China, in 2013. He is currently working toward the Ph.D. degree with the Wuhan University of Technology, Wuhan, China.

His current research interests include point cloud processing, hazard monitoring with GNSS, and safety science in mining engineering.